Applied Catalysis B: Environmental 241 (2019) 385–392

Contents lists available at ScienceDirect

Applied Catalysis B: Environmental

journal homepage: www.elsevier.com/locate/apcatb

Synthesis of Ti_xO_y nanocrystals in mild synthesis conditions for the degradation of pollutants under solar light

Hesham Hamad[1], Esther Bailón-García*, Francisco J. Maldonado-Hódar, Agustín F. Pérez-Cadenas, Francisco Carrasco-Marín, Sergio Morales-Torres

Carbon Materials Research Group, Department of Inorganic Chemistry, Faculty of Sciences, University of Granada, Avenida de Fuentenueva, s/n., ES18071 Granada, Spain

ARTICLE INFO

Keywords:
Black titania
Oxygen vacancies
Visible light photocatalysts
Band gap narrowing
Synergetic effect

ABSTRACT

Black TiO_2 is capable to absorb the entire or part of the visible spectrum improving, a priori, the photoactivity under solar irradiation. Nevertheless, black TiO_2 materials have not been able to demonstrate the expected photocatalytic activity in visible light due to the presence of a large number of recombination centers. In addition, high temperatures or pressures (> 400 °C, 20 bar) are required for the conventional synthesis and alternative methods have high energy costs which limit the capability for mass production. In this report, a novel controlled hydrolysis method has been developed to synthesize reduced black TiO_2 in mild conditions of temperature (180 °C) and pressure (8 bar). The synergetic effect of the stabilization of small crystal sizes, strong visible light absorption, band gap narrowing, Ti^{3+} defects or oxygen vacancies concentration, improved surface area and pollutant-surface interactions, significantly enhances the photocatalytic activity in the degradation of organic pollutants (Orange G) under visible light (almost totally degraded at 40 min).

1. Introduction

The industrial growth, population expansion and the increasing environmental pollution convert the water in a scarce and increasingly inaccessible resource. As consequence, the decontamination of water is one of the most serious global challenges and will be increasingly important in the future due to the appearance of new and more stable pollutants (emerging pollutants) in the water.

Different strategies have already been developed in order to combat the near future water-scarcity and deal with the increasingly restrictive legal pollution limits. Among them, the advanced oxidation processes (AOPs) have been revealed as one of the most effective methods to combat these water pollution problems [1]. These oxidation techniques are based on physicochemical processes that involve the generation and use of highly reactive radicals, mainly the hydroxyl radical ($OH^{\cdot}$), which has high effectiveness for the oxidation of pollutants [2]. Several types of AOPs are based on the *in-situ* formation of $OH^{\cdot}$ radicals by means of various chemical, photochemical, sonochemical, or electrochemical reactions. Among the photochemical methods, heterogeneous photocatalysis using TiO_2 is a simple and powerful tool, widely used and studied worldwide.

Solar photocatalysis is especially interesting for the elimination of pollutants by the use of solar energy as the sole source of energy, saving operational costs and making it a feasible route for it implementation in the industry or in the tertiary treatment of a sewage treatment plant. Thus, the use of solar energy is presented as a sustainable alternative, since the cost of installation and operation of the AOPs is relatively high. However, the high band gap of TiO_2 (3.0–3.2 eV) limits the application of solar radiation due to only the ultra-violet (UV) region of the solar spectrum can be used by titania for the photogeneration of the electron-hole pair responsible of the photocatalytic effect, resulting in insufficient utilization of solar energy (less than 5%) and low activity [3].

In order to extend the photoactivity of TiO_2 to the visible region of the solar spectrum, several approaches have been studied aiming to decrease the titania band gap, such us the introduction of doping agents or the use of sensitizers [4]. The introduction of metal (Ni, Fe, Co, Mn, Cr, …) or non-metal ions (N, C, S, I, …) narrows the bandgap of TiO_2 by producing new hybrid states which confer significant visible light absorbance toTiO_2 [5,6]. However, different problems were also detected.

* Corresponding author.
E-mail address: estherbg@ugr.es (E. Bailón-García).
[1] Present address: Fabrication Technology Research Department, Advanced Technology and New Materials Research Institute (ATNMRI), City of Scientific Research and Technology Applications (SRTA-City), New Borg El-Arab City, Alexandria, 21934, Egypt.

https://doi.org/10.1016/j.apcatb.2018.09.016
Received 9 July 2018; Received in revised form 4 September 2018; Accepted 7 September 2018
Available online 08 September 2018
0926-3373/

Metal-doped TiO_2 shows thermal instability, electron could be trapped by the metal centres decreasing the photocatalytic activity and high processing costs; whereas in non-metal doped TiO_2 the main drawbacks are the difficulty to obtain N-doped TiO_2 with high nitrogen concentration, the formation of defects which can act as recombination centres for carriers and the decrease of N concentration at the surface layer after irradiation.

Highly-dispersed TiO_2 and ZrO_2-carbon xerogels composites have been presented as a good alternative to metal and non-metal doping. Carbon matrix favours the reduction of the band gap by the stabilization of Ti^{3+} states together with the minimization of the electron-hole recombination and the improvement of the surface area increasing the number and quality of active sites, as well as the adsorption of contaminants [7,8].

Another alternative is the Ti^{3+} self-structural modified TiO_2 or so-called black titania which is capable to absorb the entire or part of the visible spectrum, resulting in black or colourful appearances. Black titania exhibits high electron carrier concentration ($\sim 7.8 \times 10^{20}$ cm^{-3}) [9] and narrow band gap of ≈ 1.5 eV [10] and consequently high absorptivity to visible/infrared light and high photocatalytic activity.

Usually, black titania is synthesised by hydrogenation of white titania [11–14], however high temperatures (400–700 °C) [15–17] or pressures (20–40 bar) [10,18,19] are required and the hydrogenation of amorphous titania precursors cannot ensure a good photocatalytic activity. Different approaches, either reduction or oxidation ones, have been made for the synthesis of black titania. Reduction of TiO_2 has been performed by hydrogenation [15–17], Ar annealing [20,21], metal-assisted (Al, Mg, Zn) [4,22,23], H_2-plasma [9], organic lithiation treatment with a lithium-amine chelating agent (Li-ethanediamine, Li-EDA) [24,25], electron beam treatment [26], proton implantation [27] and electrochemical reduction [28]. In turn, oxidation approaches consist in the incomplete oxidation of low valence Ti species such as TiO, TiH_2, $TiCl_3$ among others, in such a way high-concentration of oxygen vacancies or Ti^{3+} are obtained [29]. However, high temperatures (> 400 °C) are still required or they have high energy costs which limits the capability for mass production. Moreover, high-temperature processes easily lead to structure cracks, preventing careful nanostructure design for better performance. Hence, new strategies for black TiO_2 synthesis should be developed.

The aim of our work is to develop an alternative approach for improving the visible and infrared optical absorption by the first-time engineering of disorder titania with and without hydrogen to obtain black TiO_2 nanoparticles with controlled morphology. In the present work, black titania nanoparticles and nanofibers were synthesized in mild conditions of temperature (180 °C) and pressures (8 bar) by a stirred solvothermal method in presence of nitrogen or hydrogen. Black titania was deeply characterized and tested in the photodegradation of pollutants under visible light.

2. Materials and methods

2.1. Chemicals

Methanol (99.9%, Applichem-Panreac), acetonitrile (99.9%, Panreac), titanium (IV) isopropoxide (TTIP, > 97%, Aldrich), hexadecyltrimethylammonium bromide (CTAB, > 99%, Sigma), deionized water.

2.2. Synthesis of black titania

Black titania was prepared by a controlled hydrolysis of TTIP in methanol/acetonitrile medium using CTAB as structure-directing agent. In a typical preparation, 0.546 *g* of CTAB was added to 150 ml of methanol/acetonitrile solution. After stirring for 10 min, 1 ml of TTIP was added and then quickly transferred into a sealed stirred reactor (Parr reactor model 5500) to avoid the hydrolysis under atmospheric conditions. This mixture was heated at 60 °C under stirring (2000 rpm) and pressurized with hydrogen or nitrogen under flow in order to purge the reactor. Hydrolysis and condensation reactions occurs when adding 1 ml of deionized water in the pressurized stirred tank using a pump. After that, the flow was stopped, and the tank pressurized at 8 bar and heated at 180 °C under stirring for 1, 2, 3, 4 or 5 days. The obtained samples were centrifuged at 4000 rpm for 20 min and washed with methanol several times. These samples were denoted as TiAX, where A is H or N for H_2 or N_2, respectively and X are the days of treatments, i.e. TiH1 indicates that TiO_2 was synthesised in presence of H_2 after 1 day of treatment. White titania, TiO_2 anatase from sigma aldrich, was used as reference material.

2.3. Textural and chemical characterization

The morphology of catalysts was studied by scanning electron microscopy (SEM) using a LEO (Carl Zeiss) GEMINI-1530 microscope. HRTEM images were recorded using a FEI TITAN G2 80–300 microscope equipped with a scanning transmission electron microscopy (STEM) detector-type HAADF (high-angle annular dark-field detector), corrector of spherical aberration (CEOS), and EDX microanalysis system (Super X). This equipment has a maximum resolution of 0.8 Å (TEM) or 1.4 Å (STEM), working with an acceleration voltage of 300 kV. A small amount of well-milled sample is dispersed in ethanol under ultrasound and mounted on a 300-mesh carbon-coated cooper grid.

Textural characterization was carried out by N_2 adsorption at −196 °C using Quantachrome Autosorb-1 equipment. The BET equation and the DFT method were applied to determine the apparent surface area (S_{BET}) and mesopore volume of the samples (V_{mes}), respectively, and the Dubinin–Radushkevich equation used to calculate the micropore volume (W_0) and the mean micropore width (L_0). The total pore volume was considered as the volume of N_2 adsorbed at $P/P_0 = 0.95$.

The crystallinity was analyzed by a powder X-ray diffraction (XRD) pattern using a Bruker D8 Advance X-ray diffractometer with Cu Kα radiation at a wavelength (λ) of 1.541 Å. The 2θ angles were scanned from 20 to 70°. The average crystallite sizes (D) were estimated by the Debye-Scherer equation, $D = 0.95\lambda/\beta \cos\theta$, where θ is the diffraction angle and β is the full width at half-maximum (fwhm). The full width at half maximum (FWHM) was determined with an extrapolated baseline between the beginning (low angle side) and the end (high-angle side) of a diffraction peak with the highest intensity.

The chemical characterization of the samples was further analyzed by X-ray photoelectron spectroscopy (XPS). The spectra were obtained on a Kratos Axis Ultra-DLD X-ray photoelectron spectrometer equipped with a hemispherical electron analyzer connected to a detector DLD (delay-line detector).

Optical absorption spectra of samples were obtained on a double-beam UV–vis spectrophotometer (CARY 5E from VARIAN) equipped with a Praying Mantis diffuse reflectance accessory (DRA). The reflectance spectra were converted to absorbance by the Kulbelka–Munk (KM) method in order to calculate the band gap (Eg) of samples. Plot representations were used to calculate E_g: $(F(R)\cdot h\upsilon)^n$ *versus* E, with n = ½ for an indirect allowed transition and n = 2 for a direct allowed transition. The E_g value was obtained by extrapolating the slope to y = 0 according to the procedure used by López et al. [30].

2.4. Photocatalytic degradation procedure in presence of saturated photocatalysts

The photocatalytic activity of black TiO_2 was compared in the Orange G (OG) degradation using a glass photoreactor (inner diameter of 8.5 cm x height of 20 cm) equipped with an inner tube of 2.5 cm of diameter placed in the reactor centre, allowing to fit a visible sun lamp of 14 W (ReptoLux 2.0) inside to ensure an uniform irradiation of all solution volume. The degradation kinetic was follow by UV-

spectrometry using a UV–vis spectrophotometer (5625 Unicam Ltd., Cambridge, UK), previously calibrated.

Catalytic photodegradation was carried out using 1 mg/ml of photocatalyst, previously saturated with the dye in the dark to avoid the influence of the different adsorptive performance of each sample on the evolution of the dye concentration. After saturation, the initial dye concentration (C_0) was fitted again in all cases to 10 mg/L, and then, visible light was turned on and this time was considered as the start degradation time. At a regular interval of 10 min, equal aliquot was removed from the reactor, filtered and the OG concentration measured by UV-spectrometry.

The OG mineralization degree was followed by the evolution of total organic carbon (TOC) present in the solution during the photo-degradation experience using an analyzer Shimadzu V-CSH analyser with ASI-V autosampler and subtracting the inorganic carbon value in each sample from the total carbon value.

The Orange G adsorption isotherm on black titania was carried out also in a thermostatic bath at 298 K. For this, a volume of 25 ml with different initial concentrations of dye was placed in a flask and 0.025 g of sample was added. The flask was placed inside the thermostatic bath under shaking for 4 h to ensure the equilibrium are reached. The Orange G adsorption capacity of samples (X_{ads}, mg/g) was calculated by fitting de adsorption data to the Langmuir equation.

3. Results and discussion

3.1. Textural and chemical characterization

Black titania nanoparticles with different colours were successfully synthesized in mild experimental conditions (8 bar and 180 °C) by the controlled hydrolysis of titanium isopropoxide, either in presence of nitrogen or hydrogen. As shown in Fig. 1, TiO_2 powder was converted from white to intense gray-black by increasing the treatment time. Highlight that the dark colour is more intense in presence of H_2 in comparison with the N_2 samples, denoting a higher effectivity in the titania reduction.

The different dark colours of samples suggest excellent visible light absorption. Fig. 2 displays the diffuse reflectance spectra of the coloured titania and TiO_2-anatase as reference. A strong visible light absorption is observed for the synthesized samples regarding white TiO_2; stronger for the H_2-treated samples. Moreover, this adsorption increases by increasing the treatment time which is in line with the visual impression of the darkness of the samples. The enhanced visible light adsorption could be attributed to the effective reduction of Ti^{4+} ions of titania into Ti^{3+} by introducing oxygen vacancies [31] during the solvothermal treatment. This means that the higher is the treatment time the higher is the amount of Ti^{3+} or oxygen vacancies in the sample and thus, the effectivity of the process. This effectivity is also improved in presence of H_2 manifesting that, in spite of the soft hydrogenation conditions, titania hydrogenation takes place.

The band gap, E_g, was calculated by the Kulbelka–Munk (KM) method and results are shown in Fig. 2c. TiO_2 is an intrinsic n-type

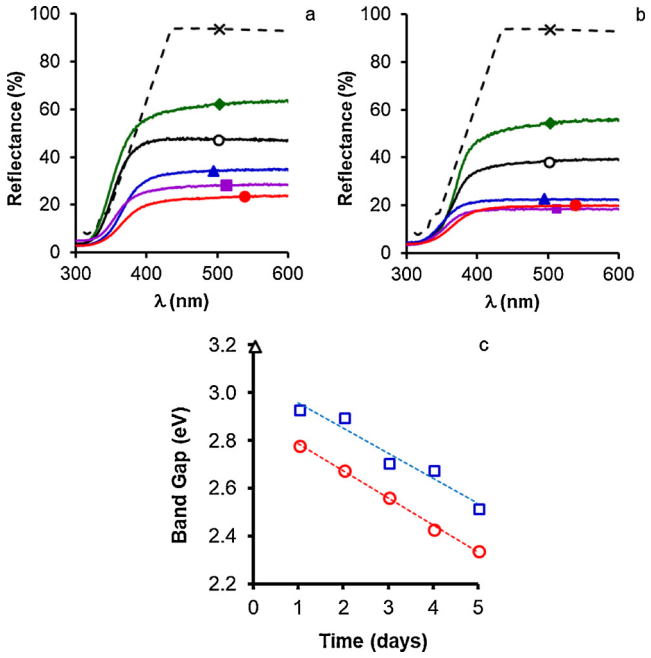

Fig. 2. Diffuse reflectance spectra of a) TiNx and b) TiHx samples in comparison with white TiO_2 (x) as reference, being x: 1 (♦), 2 (○), 3 (▲), 4 (■) or 5 (●); c) Band gap of TiNx (□), TiHx (○) and white TiO_2 (△).

semiconductor with a band gap of 3–3.2 eV. However, in the reduced state, the higher density of Ti^{3+} leads to a decrease in the band gap. As compared to white TiO_2, the optical band gap of TiNx and TiHx samples is substantially reduced (up to band gap lower than 2.3 eV) and this decrease is linearly dependent of the treatment time. Moreover, as expected, a proportional decrease of the band gap is obtained in presence of H_2 atmosphere (same slopes).

The presence of Ti^{3+} was corroborated by X-ray photoelectron spectroscopy (XPS). Fig. 3 displays the Ti2p XPS region and Table 1 collects the data obtained from XPS analysis. Only a peak centered at 459.5 eV is observed for white TiO_2 which is attributed to Ti^{4+}, whereas Ti^{3+} is the main component in colored TiO_2 (peak centered at 458.5 eV). This means that reduction occurs mainly at the surface since TiO_2 is the unique phase detected by XRD without detection of Ti_2O_3 (data shown below); and that oxidation does not take place after the exposure of samples to the air. Moreover, as expected, the % of Ti^{3+} increases with the treatment time and the hydrogen treatment improves this reduction (86 vs 92% of Ti^{3+} for TiN1 and TiH1, respectively, Table1) which corroborates the results obtained from diffuse reflectance analysis.

Regarding the O_{1s} region (Table 1), three peaks located at 529.8, 531.0, and 532.0 eV are needed, corresponding to Ti—O in surface bulk oxide lattices, acidic hydroxyl group and basic hydroxyl group, respectively [32]. Different authors have confirmed the formation of

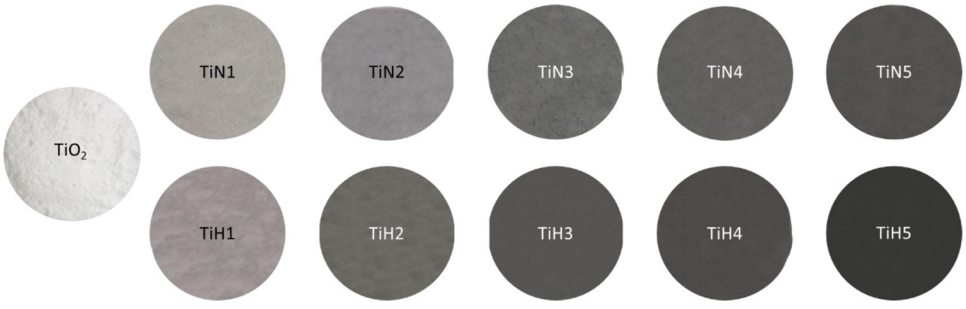

Fig. 1. Digital photographs of Ti_xO_y samples.

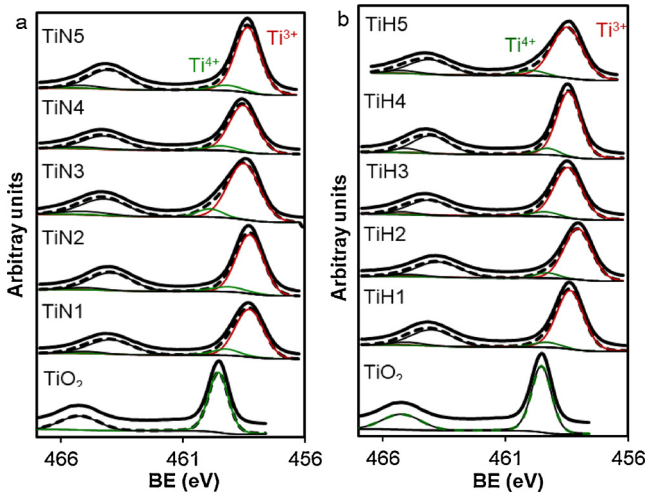

Fig. 3. Ti2p region of XPS spectra for a) TiNx and b) TiHx samples.

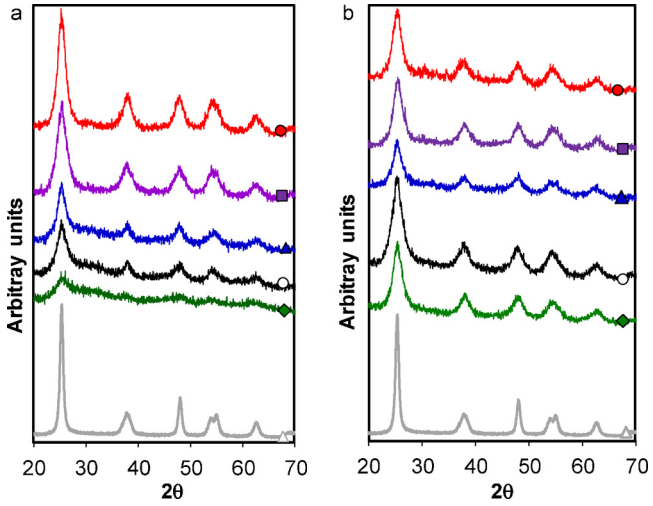

Fig. 4. XRD patterns of a) TiNx and b) TiHx samples. x: 1 (♦), 2 (○), 3 (▲), 4 (■) or 5 (●) regarding commercial TiO_2 as reference material (△).

Table 1
Ti_{2p} and O_{1s} data obtained from XPS and crystal size from XRD.

Sample	Ti_{2p}		O_{1s}			D (nm)
	BE (eV)	% peak	BE (eV)	% peak	Ti−OH/Ti−O	
TiO_2	459.5	100	530.4	80	0.25	24.6
			532.5	17		
			534.3	3		
TiN1	458.3	86.3	529.8	78	0.28	3.8
	459.2	13.7	531.2	15		
			532.2	7		
TiN2	458.2	86.5	529.7	73	0.37	3.9
	459.1	13.5	530.9	16		
			531.8	11		
TiN3	458.5	90.3	529.8	75	0.32	4.6
	459.9	9.7	531.0	19		
			532.0	6		
TiN4	458.5	91.4	529.9	74	0.35	4.7
	459.4	8.6	530.9	19		
			532.0	7		
TiN5	458.3	91.8	529.6	74	0.35	5.1
	459.2	8.2	5309	19		
			531.9	7		
TiH1	458.4	92.0	529.7	74	0.35	4.6
	459.3	8.0	530.8	18		
			531.9	8		
TiH2	458.1	92.1	529.4	72	0.39	4.3
	459.3	7.9	530.7	21		
			531.8	7		
TiH3	458.5	92.3	529.9	71	0.41	4.3
	459.4	7.7	531.1	21		
			532.2	8		
TiH4	458.4	92.6	529.8	71	0.41	4.5
	459.3	7.4	530.9	21		
			531.9	8		
TiH5	458.5	92.6	529.8	71	0.42	4.4
	459.9	7.4	531.0	22		
			532.1	7		

hydroxyl group on TiO_2 surface after hydrogenation treatments [31–34] due to the hydrogenation helping to break up Ti-O bonds on the surfaces of anatase nanocrystals by forming Ti−H and O−H bonds [35]. An increase of Ti−OH bonds (Ti−OH/Ti−O area ratio) is observed in both TiNx and TiHx samples regarding TiO_2 because of the titania reduction, but this increase is more significant in presence of H_2 corroborating again that titania hydrogenation occurs in TiHx samples during the solvothermal treatment at mild conditions.

XRD was used to investigate the crystallinity and possible phase changes of the prepared samples and results are collected in Fig. 4 and Table 1. XRD patterns of TiHx and TiNx nanoparticles was similar to that of TiO_2, except for the lower peak intensities denoting a lower crystallinity or lower crystal size, and well matched with the anatase phase TiO_2 (21-1272, JCPDS). It is clearly noticed an increase of diffraction intensities and crystal sizes in TiNx samples increasing the treatment time (Fig. 4a and Table 1) whereas in TiHx ones, crystal sizes are similar (around 4.5 nm) in all cases (Fig. 4b and Table 1). It was pointed out in literature that the intensity of the diffraction peaks decreases gradually, and peaks weaken and widened increasing the reduction effectivity of the coloured titania which are related to the amorphous phase created after the reduction process [34,36]. Usually, a surface disordered shell is observed in coloured titania due to the creation of oxygen vacancy/Ti^{3+}, surface hydroxyl groups or Ti–H bonds. This shell is amorphous and consequently, crystal sizes and diffraction intensity decrease after the reduction treatment. With that background, two considerations must to be taken into account: i) the crystallinity usually increases increasing the hydrothermal treatment time [36] and ii) the crystallinity decreases by the titania reduction [34,36]. In the TiNx series, the reduction effectivity is lower than in the case of TiHx one and consequently, the first factor is more significant than the latter and, as results, an increase in the crystallinity and particles size is observed. Conversely, in TiHx samples, the reduction efficiency is higher and thus, both factors are balanced resulting in a stabilization of the particle size.

The morphology of the black titania was analysed by scanning electron microscopy (SEM) and high-resolution transmission electron microscopy (HRTEM). Characteristic SEM and HRTEM images are collected in Fig. 5. SEM images reveals the presence of titania particles interconnected by titania nanofibers (around 60 nm of diameter), independently of the treatment time and atmosphere. In turn, HRTEM images show that the white TiO_2 is completely crystalline, displaying clearly-resolved and well-defined lattice fringes and well-ordered crystal domains of around 25 nm. In contrast, TiNx and TiHx samples display highly-disorder nanosized crystal domains (around 4 nm) with a relatively unclear fringe pattern owing to introduction of amorphous regions between crystal domains. Note that the size of the crystal domains observed by TEM corroborates the crystal sizes obtained by XRD. The distance between the adjacent lattice planes is 0.35 nm for white TiO_2, which matches the typical value for anatase. Conversely, this distance is slightly reduced to 0.30 nm for black titania suggesting the incorporation of H atoms within the host lattice.

The N_2 adsorption–desorption isotherms are depicted in Fig. 6a-b and data collected in Table 2. All samples mainly exhibit a type-IV isotherm with a hysteresis loop, indicating the mesoporous character. However, significant differences are observed between white and

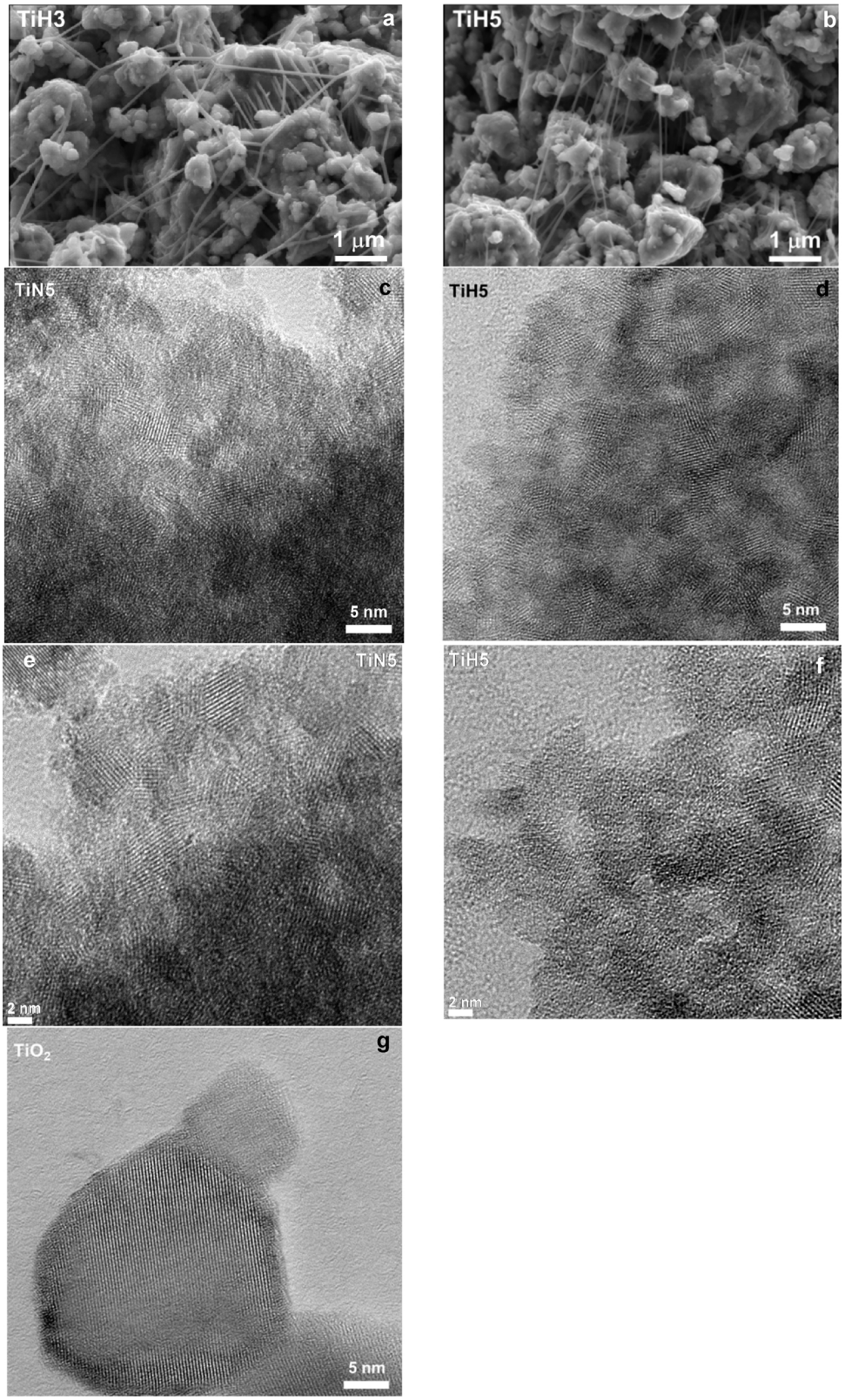

Fig. 5. Characteristic SEM (a,b) and TEM (c–g) images of the black titania.

coloured TiO_2. The hysteresis loop appears at 0.3-0.4 relative pressure for coloured titania, indicating the presence of narrow mesoporosity (3 nm, Fig. 6c-d), whereas in white TiO_2, this loop begins at higher relative pressures (0.7-0.8) indicating the presence of wider mesoporosity (20 nm, data not shown). Moreover, higher N_2 uptake at low relative pressure is observed for coloured TiO_2 indicating the development of microporosity in these cases. Note also that the textural properties are improved increasing the treatment time, i.e. the surface area increases from 133 to 191 $m^2 g^{-1}$ for N_2 serial and from 137 to 212 $m^2 g^{-1}$ for H_2 samples, increasing the treatment time from 1 to 5

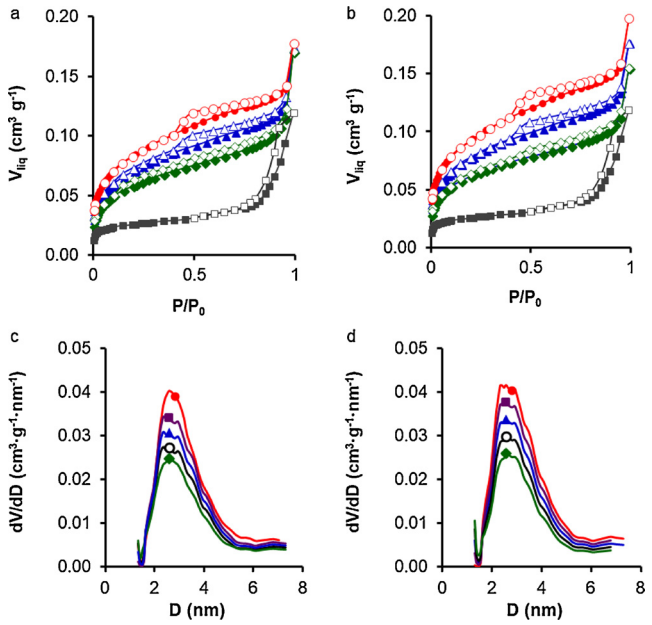

Fig. 6. N_2-isotherms and pore size distributions for TiNx (a,c) and TiHx (b,d) samples in comparison with TiO_2 (□). x: 1 (♦), 2 (○), 3 (▲), 4 (■) or 5 (●).

Table 2
Textural characterization of samples.

Sample	S_{BET} m^2/g	W_0 (N_2) cm^3/g	L_0 (N_2) nm	$V_{0.95}$ cm^3/g	V_{meso} cm^3/g
TiO_2	57	0.038	–	0.118	0.080
TiW1	133	0.052	1.81	0.114	0.063
TiW2	146	0.057	1.84	0.121	0.063
TiW3	161	0.062	1.83	0.127	0.065
TiW4	175	0.067	1.82	0.133	0.066
TiW5	191	0.075	1.89	0.139	0.064
TiH1	137	0.054	1.74	0.112	0.058
TiH2	154	0.061	1.76	0.123	0.062
TiH3	172	0.068	1.78	0.134	0.066
TiH4	190	0.074	1.79	0.145	0.071
TiH5	212	0.082	1.83	0.159	0.077

days (Table 2). The presence of H_2 during the solvothermal treatment also improves the textural properties. This improvement could be explained on the base of different crystal sizes. An increase in surface area could be attributed to a decreased crystallite size [23,37], however, similar or even larger crystal size is observed in TiHx and TiNx series increasing the treatment time. This seems to indicate that the reduction effectivity and defective TiO_{2-x} play and important role in the texture of samples. The amorphous titania typically shows BET surface areas higher than the crystalline counterparts [38,39]. This defective phase increases with the effectiveness of the titania reduction method and consequently, with the treatment time. Therefore, the present synthesis method improves the porous texture of coloured titania regarding white one; significantly affects the pore structure and surface area of the obtained TiO_{2-x} samples, and consequently, this improved porous structure must have a beneficial effect in the photocatalytic performance of coloured TiO_2.

3.2. Photocatalytic activity

The photocatalytic activity of coloured TiO_2 was evaluated towards the degradation of an industrial textile dye, Orange G (OG), under a low power artificial visible light (14 W). Prior to the photocatalytic test, catalysts were saturated with OG in dark in order to avoid adsorption interferences and the initial concentration fitted in 10 mg/l. In Fig. 7,

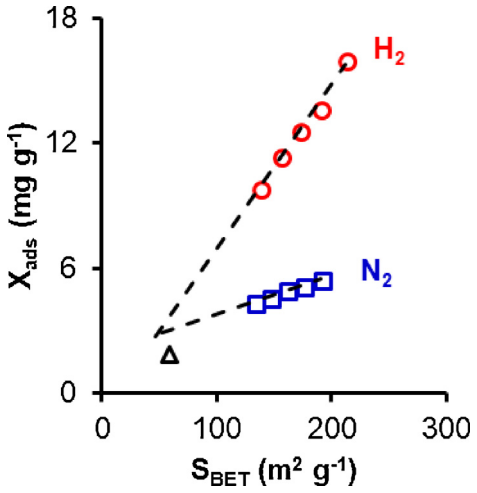

Fig. 7. Orange G adsorption capacity of samples as a function of surface area. TiHx (○), TiNx (□) and TiO_2 (Λ).

the Orange G adsorption capacity of samples was plotted as a function of the specific surface area. As could be expected, the adsorption capacity linearly increases with the surface area for both TiNx and TiHx samples, but significant differences are observed between them; much higher absorption capacity is obtained in TiHx samples despite similar surface area. To explain this fact, two factors must to be taken into account; i) the specific surface area for the adsorption of the pollutant and ii) the electrostatic interactions of the pollutant with the surface. Zeta potential results have demonstrated an increased positive charge on titania surface increasing the Ti^{3+} defects or oxygen vacancies on the surface [40,41]. The adsorption of Orange G, a negatively charged molecule, could be favoured on positively charged oxygen vacancies. It has been pointed out that the adsorption of cationic dyes (such as methylene blue) is favoured increasing de pH of the solution due to for pH's higher than the point zero charge (pzc) of titania, the surface becomes negatively charged and its adsorption is favoured on a negatively charged surface. By contrast, OG has its adsorption inhibited by high pH's because of its negatively charged sulfonate, SO_3^- function [42,43]. In a similar way, the increase of oxygen vacancies on the surface of coloured titania creates an electron deficiency on the surface and thus, a positively charged titania surface, favouring the interaction with anionic dyes (such as Orange G). Consequently, this adsorption is favoured on the TiHx samples regarding TiNx due to the development of a more defective titania surface in presence of H_2 (Ti^{3+}/oxygen vacancies observed by XPS). Note that the adsorption capacity of white TiO_2 is lower than the expected according with TiNx and TiHx linear series due to the absence or low amount of oxygen vacancies and thus, the null or scarce contribution of the specific interactions in the adsorption capacity. Mineralization of dye was followed by the Total Organic Carbon (TOC) measurement and total degradation was found in all cases, and consequently, intermediary products were not analyzed.

Fig. 8 shows the removal of OG as a function of the irradiation time. As it can be observed, very low degradation is obtained using white TiO_2 as catalyst due to its high band gap (3.2 eV) with limits the activity under visible light. Conversely, activity is observed using colored TiO_2 as catalysts which increases increasing the solvothermal treatment time. This increasing activity is related with the enhanced visible light adsorption attributed to the effective reduction of Ti^{4+} ions of titania into Ti^{3+} by introducing oxygen vacancies. A linear relationship between the time needed to achieve the 50% of Orange G degradation ($t_{0.5}$) and the photocatalyst band gap is obtained inside each serial (Fig. 9). Nevertheless, differences between TiNx and TiHx series are again observed. Time longer that 200 min are needed for the complete degradation of Orange G in TiNx serial whereas total degradation is

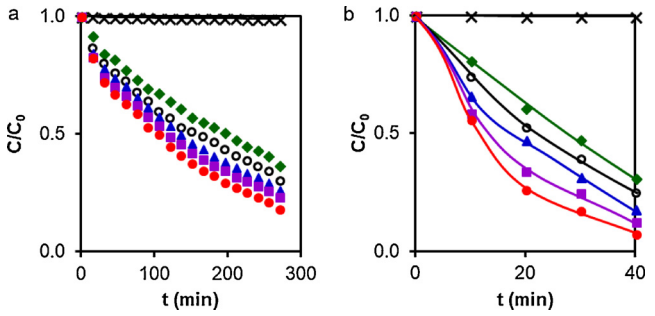

Fig. 8. Kinetic of Orange G photocatalytic degradation using a) TiNx and b) TiHx samples in comparison with white TiO_2 (x). x: 1 (♦), 2 (○), 3 (▲), 4 (■) or 5 (●).

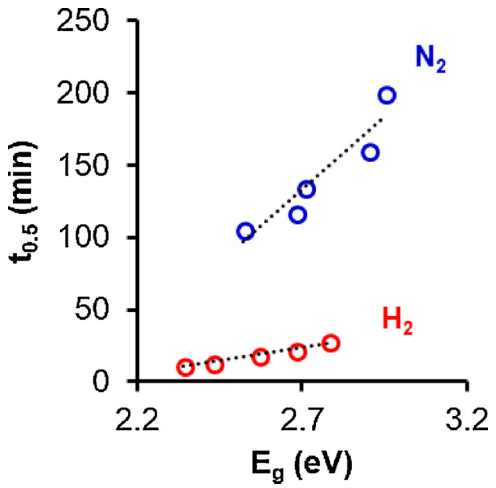

Fig. 9. Relationship between the time needed to achieve the 50% of Orange G degradation ($t_{0.5}$) and the photocatalyst band gap. TiHx (○), TiNx (□) and TiO_2 (Δ).

obtained after 80 min of reaction using TiHx as catalysts. It is true that an activity improvement must be observed in TiHx samples due to the lower band gap of these samples, but the improvement is much higher than the expected considering the obtained band gap in comparison with TiNx serial. In these sense, additional factors could contribute to this enhanced behaviour: surface area and specific interactions. It is well known that the photoactivity performance is strongly depended on the adsorption capacity of the photocatalyst, as it is known that the photocatalytic reaction occurs on the photocatalyst surface. As has been commented above, the absorption capacity of TiHx samples is enhanced regarding TiNx ones due to the improvement of surface area and electrostatic interactions surface-dye, and thus, the activity is highly improved.

The surface disorder is another important factor to consider explaining the better activity of coloured titania. It has been demonstrated that the improved photoactivity of black TiO_2 results from a synergistic effect of the oxygen vacancies on core and surface disorder, that is the surface localization of defects [44]. In this sense, it was observed that decreasing the relative concentration ratio of bulk defects to surface defects in TiO_2 nanocrystals significantly improves the charge separation efficiency and, thus, enhances the photoactivity [45]. Considering that, the high concentration of Ti^{3+} into the surface of the synthesized as it has been pointed out by TEM and XPS, improves the photocatalytic performance of both TiNx and TiHx catalysts. The highest concentration of surface defects (denoted by XPS) and the highest surface area of TiHx samples results in a highest overall surface disorder resulting in a better photoactivity. So, in TiHx catalysts, the combination of different factors as improved band gap, surface area and specific interactions and the surface localization of defects results in a superior photoactivity.

In brief, TiH5 present the best photocatalytic performance. Orange G is almost totally degraded after a very short time of reaction (lower than 40 min) under visible irradiation. This excellent behaviour is due to the optimization of a series of factors by the proposed solvothermal synthesis method with the benefit of softer experimental conditions in comparison with other methods described in bibliography in which temperatures higher than 400 °C or pressures higher than 20 bars are required. These factors are: i) the stabilization of low crystal sizes (lower than 5 nm) which improves the accessible surface area for the pollutants adsorption and minimizes the electron-hole recombination probability. In these sense, in small TiO_2 nanoparticles, the distance that the photogenerated electrons and holes need to travel to surface reaction sites is reduced, thereby reducing the recombination probability; ii) Strong visible light absorption and Band gap reduction. Oxygen vacancies/Ti^{3+} species confer a black colour to TiO_2 and creates new hybrid states in the band gap, which narrows the band gap and enhances significant visible light adsorption; iii) Ti^{3+} defects or oxygen vacancies increase positive charge on titania surface improving the electrostatic interaction of Orange G, a negatively charged molecule, with the positively charged TiO_2 surface; and iv) the surface localization of defects which significantly improves the electron-hole separation efficiency and thus, significantly enhancing the photocatalytic efficiency.

4. Conclusions

Coloured TiO_2 was successfully synthesized by the controlled hydrolysis of a titanium alkoxide under controlled atmosphere (N_2 or H_2) with the benefit of softer synthesis conditions in comparison with other methods described in bibliography in which temperatures higher than 400 °C or pressures higher than 20 bars are required. The colour of samples changes to more intense dark depending of the treatment time suggesting excellent visible light absorption. The material possesses an optimum band gap and visible light adsorption, Ti^{3+}/ oxygen vacancies concentration, surface defects, crystal size, surface area and improved pollutant-surface interactions which significantly enhances the photoactivity under visible light. An industrial textile dye, Orange G, was selected as target molecule. The OG adsorption is controlled by the specific surface area but also the electrostatic interactions of the pollutant with the surface. The increasing positive charge on titania surface due to the increase of Ti^{3+} or oxygen vacancies on the surface improves the electrostatics interactions with Orange G, a negatively charged molecule, and favour its adsorption. The exceptional photocatalytic behaviour of coloured TiO_2 could be related with the different optimized properties of the samples: i) the stabilization of low crystal sizes (lower than 5 nm) which improves the accessible surface area for the pollutants adsorption and minimizes the electron-hole recombination probability; ii) the strong visible light absorption and band gap reduction and iii) Ti^{3+} defects or oxygen vacancies increase positive charge on titania surface improving the electrostatic interaction of Orange G favouring its absorption and degradation.

Acknowledgements

This research is supported by the FEDER and Spanish projects CTQ2013-44789-R (MINECO) and P12-RNM-2892 (Junta de Andalucía). H. Hamad acknowledges a predoctoral fellowship from Erasmus Mundus (Al-Idrisi II). E. Bailón-García is grateful to MINECO for her postdoctoral fellowship (FJCI-2015-23769). S. Morales-Torres acknowledges the financial support from University of Granada (Reincorporación Plan Propio).

References

[1] M.A. Oturan, J.J. Aaron, Advanced oxidation processes in water/wastewater

treatment: principles and applications. A review, Crit. Rev. Environ. Sci. Technol. 44 (2014) 2577–2641, https://doi.org/10.1080/10643389.2013.829765.
[2] C. Comninellis, A. Kapalka, S. Malato, S.A. Parsons, I. Poulios, D. Mantzavinos, Advanced oxidation processes for water treatment: advances and trends for R&D, J. Chem. Technol. Biotechnol. 83 (2008) 769–776, https://doi.org/10.1002/jctb.1873.
[3] M. Pelaez, N.T. Nolan, S.C. Pillai, M.K. Seery, P. Falaras, A.G. Kontos, P.S.M. Dunlop, J.W.J. Hamilton, J.A. Byrne, K. O'Shea, M.H. Entezari, D.D. Dionysiou, A review on the visible light active titanium dioxide photocatalysts for environmental applications, Appl. Catal. B Environ. 125 (2012) 331–349, https://doi.org/10.1016/j.apcatb.2012.05.036.
[4] R. Daghrir, P. Drogui, D. Robert, Modified TiO_2 for environmental photocatalytic applications: a review, Ind. Eng. Chem. Res. 52 (2013) 3581–3599, https://doi.org/10.1021/ie303468t.
[5] J. Zhang, Y. Wu, M. Xing, S.A.K. Leghari, S. Sajjad, Development of modified N-doped TiO_2 photocatalyst with metals, nonmetals and metal oxides, Energy Environ. Sci. 3 (2010) 715–726, https://doi.org/10.1039/B927575D.
[6] M.A. Henderson, A surface science perspective on TiO_2 photocatalysis, Surf. Sci. Rep. 66 (2011) 185–297, https://doi.org/10.1016/j.surfrep.2011.01.001.
[7] E. Bailón-García, A. Elmouwahidi, F. Carrasco-Marín, A.F. Pérez-Cadenas, F.J. Maldonado-Hódar, Development of carbon-ZrO_2 composites with high performance as visible-light photocatalysts, Appl. Catal. B Environ. 217 (2017) 540–550, https://doi.org/10.1016/j.apcatb.2017.05.090.
[8] E. Bailón-García, A. Elmouwahidi, M.A. Álvarez, F. Carrasco-Marín, A.F. Pérez-Cadenas, F.J. Maldonado-Hódar, New carbon xerogel-TiO_2 composites with high performance as visible-light photocatalysts for dye mineralization, Appl. Catal. B Environ. 201 (2017) 29–40, https://doi.org/10.1016/j.apcatb.2016.08.015.
[9] Z. Wang, C. Yang, T. Lin, H. Yin, P. Chen, D. Wan, F. Xu, F. Huang, J. Lin, X. Xie, M. Jiang, H-doped black titania with very high solar absorption and excellent photocatalysis enhanced by localized surface plasmon resonance, Adv. Funct. Mater. 23 (2013) 5444–5450, https://doi.org/10.1002/adfm.201300486.
[10] X. Chen, L. Liu, P.Y. Yu, S.S. Mao, Increasing solar absorption for photocatalysis with black hydrogenated titanium dioxide nanocrystals, Science 331 (2011) 746–750, https://doi.org/10.1126/science.1200448.
[11] X. Chen, L. Liu, F. Huang, Black titanium dioxide (TiO_2) nanomaterials, Chem. Soc. Rev. 44 (2015) 1861–1885, https://doi.org/10.1039/c4cs00330f.
[12] M.A. Green, J. Xu, H. Liu, J. Zhao, K. Li, L. Liu, H. Qin, Y. Zhu, D. Shen, X. Chen, Terahertz absorption of hydrogenated TiO_2 nanoparticles, Mater. Today Phys. 4 (2018) 64–69, https://doi.org/10.1016/j.mtphys.2018.04.001.
[13] T. Xia, C. Zhang, N.A. Oyler, X. Chen, Hydrogenated TiO_2 nanocrystals: a novel microwave absorbing material, Adv. Mater. 25 (2013) 6905–6910, https://doi.org/10.1002/adma.201303088.
[14] T. Xia, X. Chen, Revealing the structural properties of hydrogenated black TiO_2 nanocrystals, J. Mater. Chem. A 1 (2013) 2983–2989, https://doi.org/10.1039/c3ta01589k.
[15] Y. Zhu, D. Liu, M. Meng, H_2 spillover enhanced hydrogenation capability of TiO_2 used for photocatalytic splitting of water: a traditional phenomenon for new applications, Chem. Commun. 50 (2014) 6049–6051, https://doi.org/10.1039/C4CC01667J.
[16] X. Jiang, Y. Zhang, J. Jiang, Y. Rong, Y. Wang, Y. Wu, C. Pan, Characterization of oxygen vacancy associates within hydrogenated TiO_2: a positron annihilation study, J. Phys. Chem. C 116 (2012) 22619–22624, https://doi.org/10.1021/jp307573c.
[17] A. Naldoni, M. Allieta, S. Santangelo, M. Marelli, F. Fabbri, S. Cappelli, C.L. Bianchi, R. Psaro, V. Dal Santo, Effect of nature and location of defects on bandgap narrowing in black TiO_2 nanoparticles, J. Am. Chem. Soc. 134 (2012) 7600–7603, https://doi.org/10.1021/ja3012676.
[18] J. Qiu, S. Li, E. Gray, H. Liu, Q.-F. Gu, C. Sun, C. Lai, H. Zhao, S. Zhang, Hydrogenation synthesis of blue TiO_2 for high-performance lithium-ion batteries, J. Phys. Chem. C 118 (2014) 8824–8830, https://doi.org/10.1021/jp501819p.
[19] N. Liu, C. Schneider, D. Freitag, M. Hartmann, U. Venkatesan, J. Müller, E. Spiecker, P. Schmuki, Black TiO_2nanotubes: cocatalyst-free open-circuit hydrogen generation, Nano Lett. 14 (2014) 3309–3313, https://doi.org/10.1021/nl500710j.
[20] M. Salari, K. Konstantinov, H.K. Liu, Enhancement of the capacitance in TiO_2 nanotubes through controlled introduction of oxygen vacancies, J. Mater. Chem. 21 (2011) 5128, https://doi.org/10.1039/c0jm04085a.
[21] M. Tian, M. Mahjouri-Samani, G. Eres, R. Sachan, M. Yoon, M.F. Chisholm, K. Wang, A.A. Puretzky, C.M. Rouleau, D.B. Geohegan, G. Duscher, Structure and formation mechanism of black TiO_2 nanoparticles, ACS Nano 9 (2015) 10482–10488, https://doi.org/10.1021/acsnano.5b04712.
[22] S.S. Ataei, S.J. Hashemifar, M.R. Mohammadizadeh, First-principles insights into role of hydrogen atom in black titania, Comput. Mater. Sci. 139 (2017) 84–88, https://doi.org/10.1016/j.commatsci.2017.07.014.
[23] A. Sinhamahapatra, J.-P. Jeon, J.-S. Yu, A new approach to prepare highly active and stable black titania for visible light-assisted hydrogen production, Energy Environ. Sci. 8 (2015) 3539–3544, https://doi.org/10.1039/C5EE02443A.
[24] K. Zhang, S. Ravishankar, M. Ma, G. Veerappan, J. Bisquert, F. Fabregat-Santiago, J.H. Park, Overcoming charge collection limitation at solid/liquid interface by a controllable crystal deficient overlayer, Adv. Energy Mater. 7 (2017) 1600923, , https://doi.org/10.1002/aenm.201600923.
[25] K. Zhang, L. Wang, J.K. Kim, M. Ma, G. Veerappan, C.L. Lee, K.J. Kong, H. Lee, J.H. Park, An order/disorder/water junction system for highly efficient co-catalyst-free photocatalytic hydrogen generation, Energy Environ. Sci. 9 (2016) 499–503, https://doi.org/10.1039/c5ee03100a.
[26] M.M. Khan, S.A. Ansari, D. Pradhan, M.O. Ansari, D.H. Han, J. Lee, M.H. Cho, Band gap engineered TiO2 nanoparticles for visible light induced photoelectrochemical and photocatalytic studies, J. Mater. Chem. A 2 (2014) 637–644, https://doi.org/10.1039/C3TA14052K.
[27] N. Liu, V. Häublein, X. Zhou, U. Venkatesan, M. Hartmann, M. MačKović, T. Nakajima, E. Spiecker, A. Osvet, L. Frey, P. Schmuki, "Black" TiO_2 nanotubes formed by high-energy proton implantation show noble-metal-co-catalyst free photocatalytic H_2-evolution, Nano Lett. 15 (2015) 6815–6820, https://doi.org/10.1021/acs.nanolett.5b02663.
[28] H. Li, Z. Chen, C.K. Tsang, Z. Li, X. Ran, C. Lee, B. Nie, L. Zheng, T. Hung, J. Lu, B. Pan, Y.Y. Li, Electrochemical doping of anatase TiO2 in organic electrolytes for high-performance supercapacitors and photocatalysts, J. Mater. Chem. A 2 (2014) 229–236, https://doi.org/10.1039/C3TA13963H.
[29] X. Liu, G. Zhu, X. Wang, X. Yuan, T. Lin, F. Huang, Progress in black titania: a new material for advanced photocatalysis, Adv. Energy Mater. 6 (2016), https://doi.org/10.1002/aenm.201600452.
[30] R. López, R. Gómez, Band-gap energy estimation from diffuse reflectance measurements on sol–gel and commercial TiO_2: a comparative study, J. Solgel Sci. Technol. 61 (2012) 1–7, https://doi.org/10.1007/s10971-011-2582-9.
[31] G. Zhu, J. Xu, W. Zhao, F. Huang, Constructing black titania with unique nanocage structure for solar desalination, ACS Appl. Mater. Interfaces 8 (2016) 31716–31721, https://doi.org/10.1021/acsami.6b11466.
[32] C.Y. Wu, K.J. Tu, J.P. Deng, Y.S. Lo, C.H. Wu, markedly enhanced surface hydroxyl groups of TiO_2 nanoparticles with superior water-dispersibility for photocatalysis, Mater. (Basel) 10 (2017), https://doi.org/10.3390/ma10050566.
[33] G. Wang, H. Wang, Y. Ling, Y. Tang, X. Yang, R.C. Fitzmorris, C. Wang, J.Z. Zhang, Y. Li, Hydrogen-treated TiO_2 nanowire arrays for photoelectrochemical water splitting, Nano Lett. 11 (2011) 3026–3033, https://doi.org/10.1021/nl201766h.
[34] X. Liu, B. Hou, G. Wang, Z. Cui, X. Zhu, X. Wang, Black titania/graphene oxide nanocomposite films with excellent photothermal property for solar steam generation, J. Mater. Res. 33 (2018) 674–684, https://doi.org/10.1557/jmr.2018.25.
[35] C. Fan, C. Chen, J. Wang, X. Fu, Z. Ren, G. Qian, Z. Wang, black hydroxylated titanium dioxide prepared via ultrasonication with enhanced photocatalytic activity, Sci. Rep. 5 (2015) 11712, https://doi.org/10.1038/srep11712.
[36] J. Su, Y. Liang, S. Yunfei, S. Shuhua, J. Song, Z. Zhuojing, Effects of hydrothermal treatment on the properties of nanoapatite crystals, Int. J. Nanomed. 7 (2012) 5151, https://doi.org/10.2147/IJN.S34077.
[37] N. Muhd Julkapli, S. Bagheri, Applications of titania as a heterogeneous catalyst for degradation of landfill leachates, in: N. Muhd Julkapli, S. Bagheri (Eds.), Nanocatalysts Environ. Appl. Springer International Publishing, Switzerland, 2018, , https://doi.org/10.1007/978-3-319-69557-0.
[38] T. Fröschl, U. Hörmann, P. Kubiak, G. Kučerová, M. Pfanzelt, C.K. Weiss, R.J. Behm, N. Hüsing, U. Kaiser, K. Landfester, M. Wohlfahrt-Mehrens, High surface area crystalline titanium dioxide: potential and limits in electrochemical energy storage and catalysis, Chem. Soc. Rev. 41 (2012) 5313–5360, https://doi.org/10.1039/c2cs35013k.
[39] K. Kaur, C.V. Singh, Amorphous TiO_2as a photocatalyst for hydrogen production: a DFT study of structural and electronic properties, Energy Procedia 29 (2012) 291–299, https://doi.org/10.1016/j.egypro.2012.09.035.
[40] V.E. Alexandrov, E.A. Kotomin, J. Maier, R.A. Evarestov, First-principles study of bulk and surface oxygen vacancies in $SrTiO_3$ crystal, Eur. Phys. J. B 72 (2009) 53–57, https://doi.org/10.1140/epjb/e2009-00339-4.
[41] H. Qin, Y. Bian, Y. Zhang, L. Liu, Z. Bian, Effect of Ti (III) surface defects on the process of photocatalytic reduction of hexavalent chromium, Chinese J. Chem. 35 (2017) 203–208, https://doi.org/10.1002/cjoc.201600578.
[42] S. Asuha, X.G. Zhou, S. Zhao, Adsorption of methyl orange and Cr(VI) on mesoporous TiO_2 prepared by hydrothermal method, J. Hazard. Mater. 181 (2010) 204–210, https://doi.org/10.1016/j.jhazmat.2010.04.117.
[43] H. Lachheb, E. Puzenat, A. Houas, M. Ksibi, E. Elaloui, C. Guillard, J.M. Herrmann, Photocatalytic degradation of various types of dyes (Alizarin S, Crocein Orange G, Methyl Red, Congo Red, Methylene Blue) in water by UV-irradiated titania, Appl. Catal. B Environ. 39 (2002) 75–90, https://doi.org/10.1016/S0926-3373(02)00078-4.
[44] K. Zhang, J.H. Park, Surface localization of defects in black TiO_2: enhancing photoactivity or reactivity, J. Phys. Chem. Lett. 8 (2017) 199–207, https://doi.org/10.1021/acs.jpclett.6b02289.
[45] M. Kong, Y. Li, X. Chen, T. Tian, P. Fang, F. Zheng, X. Zhao, Tuning the relative concentration ratio of bulk defects to surface defects in TiO_2 nanocrystals leads to high photocatalytic efficiency, J. Am. Chem. Soc. 133 (2011) 16414–16417, https://doi.org/10.1021/ja207826q.